Structures and stabilities of small carbon interstitial clusters in cubic silicon carbide

Chao Jiang[*], Dane Morgan[†], and Izabela Szlufarska[‡]

Department of Materials Science and Engineering, University of Wisconsin, Madison, WI 53706, USA

Abstract

Knowledge of the configurations and stabilities of defect clusters in SiC is important for understanding radiation damage in this material relevant to its nuclear and electronic applications. Such information is however often difficult to obtain experimentally. In this study, we perform Monte-Carlo basin-hopping simulations with both empirical potential and density functional theory (DFT) calculations to search for the ground state (GS) configurations of small carbon interstitial clusters and carbon-antisite-based defects in cubic SiC (3C-SiC). Educated guesses of possible GS configurations have also been made. Our new approach can successfully identify many hitherto unknown GS and energetically highly competitive metastable structures. For carbon penta- and hexa-interstitials, the GS structures predicted by DFT and empirical potential differ, and the plausible origin of this discrepancy is discussed from the chemical bonding point of view. Surprisingly, the GS structures of large carbon interstitial clusters in SiC are disjointed and composed of di- and tri-interstitial clusters as fundamental building blocks. Based on the present results, a possible mechanism for the carbon tri-interstitial defect to grow into the extended {111} planar interstitial defects observed in neutron-irradiated 3C-SiC is proposed. Furthermore, we show that C interstitial clusters can get trapped at a carbon antisite and form very stable complexes in SiC.

[*]cjiang32@wisc.edu (CJ), [†]ddmorgan@wisc.edu (DM), [‡]szlufarska@wisc.edu (IS)

1. Introduction

Cubic silicon carbide (3C-SiC) with a zinc-blende crystal structure is a promising structural and cladding material for nuclear fission and fusion reactors due to its excellent mechanical strength, high-temperature stability, and low neutron capture cross section [1, 2]. Its hexagonal polytype (4H-SiC) is also a wide band-gap semiconductor for high-temperature, high-power, and high-frequency devices [3, 4]. Under thermodynamic equilibrium conditions, the concentrations of point defects in SiC are extremely low due to their high formation energies [5]. However, when exposed to displacive radiation environments (e.g., during neutron irradiation or ion implantation), lattice defects are created in amounts significantly greater than their equilibrium concentrations. If left unchecked, the accumulation of irradiation-induced lattice damage can lead to unwanted microstructural changes such as crystalline-to-amorphous transformation [6, 7] and volume swelling [8], as well as degradation of the mechanical [9, 10] and electrical [11] properties of SiC. Therefore, to fully exploit the potential of SiC for both nuclear and electronic applications, a fundamental understanding of the production and long-time evolution of radiation damage in this material is crucial.

Radiation damage is an inherently multiscale phenomenon that spans many time and length scales [12-14]. Irradiation by light particles such as electrons creates single Frenkel defects (interstitial-vacancy pairs). In cubic SiC, the average threshold displacement energy (i.e. the minimum kinetic energy necessary to create a stable Frenkel pair) for the C and Si sublattice was calculated to be 19 and 38 eV, respectively [15]. For C atoms, a threshold displacement energy of 21.8 eV was experimentally observed in 6H-SiC [16]. In contrast, heavy ions and neutrons produce cascade displacement damage.

The primary damage in SiC due to collision cascades has been investigated using molecular dynamics (MD) simulations [17, 18] with a modified Tersoff [19] potential. It was found that defects surviving 10 and 50 keV Si displacement cascades in SiC are mostly single point defects, including C and Si Frenkel pairs as well as antisite defects on both Si and C sublattices. For high-energy cascades, multiple subcascades can lead to in-cascade formation of interstitial clusters containing up to four interstitials [18]. Over longer time scales, irradiation-induced point defects and their complexes can migrate and recombine harmlessly with their anti-defects (e.g., vacancy-interstitial recombination [20-22]), annihilate at internal sinks such as grain boundaries [23, 24], or aggregate with each other to form larger defect clusters such as interstitial Frank loops and voids. Since such processes are inaccessible to MD simulations due to their intrinsic time-scale limitations (ps to ns), higher-level modeling techniques such as object kinetic Monte Carlo (OKMC) [13, 25] and mean field rate theory model [25, 26] are needed to extend the simulation time and length scales to the mesoscale regime.

For a predictive multiscale modeling of defect kinetics in irradiated SiC, detailed knowledge of the diffusion, recombination, clustering, and dissociation mechanisms of point defects and their complexes is critical. For SiC, explicit consideration of defect clustering is particularly important since point defects are known to have a strong tendency to agglomerate in this material. For example, the binding energy between two C interstitials in SiC is around 5 eV [27-29], which is over six-fold larger than that between two Fe interstitials in bcc Fe (0.8 eV [13]). The formation of defect clusters can strongly influence damage evolution in irradiated materials, as has been demonstrated by Ortiz

and Caturla [25] using bcc Fe as an example. It was shown that the damage recovery process becomes kinetically hindered when point defects are immobilized into clusters.

In typical OKMC simulations, defect clusters are assumed to be point-like and their detailed atomic configurations are ignored. Consequently, only the most stable (hence thermodynamically most probable) defect configurations are considered. For covalently bonded materials such as SiC, the situation is however more complicated since rearrangements of defect structures can be kinetically difficult. It is thus likely that metastable defect configurations can co-exist with the stable ones even at high temperatures, leading to different mechanisms of their migration and reaction.

The purpose of the present study is to systematically investigate the structures and stabilities of small carbon interstitial clusters (I_n, cluster size n up to 6) as well as carbon interstitial clusters centered on an antisite defect ($(C_n)_{Si}$, n up to 4) in cubic SiC using a combination of empirical potential and density functional theory (DFT) modeling techniques. Findings of both ground-state (GS) and energetically competitive metastable defect configurations are presented. Here, we focus on the clustering of C interstitials since C Frenkel Pairs are produced in much higher quantities than Si Frenkel Pairs during irradiation [17, 18] and the C interstitials are highly mobile (migration barriers are 0.74 eV [30], 0.5 eV [22]). The abundance of mobile C interstitials means that clusters of C interstitials are likely to be important defects over a wide-range of temperatures and irradiation conditions. Our search unveils new GS structures for carbon penta- and hexa-interstitial clusters as well as tetra-carbon antisite that are previously unknown. Surprisingly, even for small clusters such as carbon di-, tri- and tetra-interstitials, our search identifies many energetically highly competitive metastable structures that were

not found in our previous study [29]. These new structures are likely to be observed experimentally because of their large stability. Based on the present results, we propose a possible mechanism for the carbon tri-interstitial defect to grow into the experimentally observed planar interstitial clusters lying on {111} planes in neutron-irradiated 3C-SiC [31-33]. The interactions between C interstitial clusters and a C antisite have also been investigated in this study.

2. Global optimization strategy

The determination of the GS geometry of a cluster of atoms is a formidable global optimization task due to the enormous number of local minima on the potential energy surface (PES), which tends to grow exponentially with cluster size [34-36]. In the case of defect clusters embedded in a crystal, the situation is even more complicated due to the interplay of electronic and elastic interactions of the defect cluster with the underlying lattice, which interactions can be long range in nature. Large supercells are needed to minimize artificial defect-defect interactions due to the periodic boundary conditions, especially for large clusters. Furthermore, in SiC, the energy barriers for transitions between different defect cluster configurations are very high, which can prevent a satisfactory sampling of the PES by MD simulations. From the DFT calculated cohesive energies (see Sec. 3.3 for computational details) of diamond and cubic SiC divided by the total number of nearest-neighbor bonds (2 per atom), we estimate that breaking a C-C and Si-C single bond would cost an energy of 4.4 and 3.6 eV, respectively. This estimate is of course approximate because it ignores any bond-order effects. However, it does illustrate that bond breaking and reconfiguration in SiC is a rare event on the time scales of classical MD simulations.

In our previous study [29], we employed a combination of random structure searching [37-39] and MD simulated annealing [35, 40-42] with empirical potential, followed by DFT structural optimizations, to search for the GS defect cluster geometries in SiC. By performing simulated annealing runs starting from many randomly generated defect cluster configurations, it was assumed that an adequate exploration of the PES can be achieved, which is essential for guaranteeing the finding of the true global minimum. While the random sampling approach worked well for small defect clusters and successfully discovered the GS geometries of carbon di-, tri- and tetra-interstitial clusters in SiC [29], it quickly becomes ineffective for treating larger defect clusters (n>4) due to the exponentially increasing complexity of their energy landscapes with n.

To overcome the inefficiency of the combined random configuration sampling and simulated annealing approach developed in our previous study, here we employ a basin-hopping method [43, 44] that has been shown to be highly effective for global optimizations problems. One big advantage of this method is that it can directly ‘‘hop’’ between nearby local minima without having to overcome the high transition barriers separating them, which is particularly important for our study. Basin hopping is initially performed with less accurate but computationally more efficient empirical potential to extensively explore the PES. Among the pool of symmetrically distinct structures found, around 40 of them with low energies (not necessarily the lowest-energy structure) are selected as best candidates. While studies with empirical potentials provide an excellent guidance for finding stable cluster structures, these potentials are approximate in nature and alone can lead to artifacts. We therefore complement this analysis by making several educated guesses of possible GS configurations based on our physical intuitions as well

as based on cluster configurations that are known to exist in materials with diamond crystal structure. Subsequently, we carry out DFT calculations to determine which of the candidate configurations is energetically the most favorable for a given defect cluster type. In addition, for each of the lowest-energy structures found, we test its stability by using it as the starting configuration of a small number (around 100) of DFT-based basin hopping steps. As will be shown, our approach not only leads to the discovery of the true GS structures of carbon penta- and hexa-interstitial clusters as well as tetra-carbon antisite, but also reveals many interesting low-energy metastable configurations. It is worth noting that many of these structures can only be discovered by DFT calculations, but not by simulations based on empirical potential.

3. Computational details

3.1. Monte Carlo basin hopping

We perform ground state search using the basin-hopping algorithm, also referred to as Monte Carlo (MC) with local minimization [43, 44]. Through local energy minimizations, the original PES is transformed into a simplified one that resembles a multidimensional staircase, with each step corresponding to a "basin of attraction" surrounding a local minimum. By doing so, the system can directly ''hop'' between local minima on the PES without having to overcome the high barriers between them. This is particularly important for an adequate sampling the PESs of defect clusters in SiC since the transition barriers can be rather high. The transformed PES is explored using canonical MC simulations at a constant temperature with the Metropolis algorithm. When the temperature is chosen too high, many up-hill MC moves will be accepted and the basin-hopping method becomes similar to a random walk on the PES. Conversely, when

the temperature is set too low, the system can easily get stuck in the wrong local minimum without possibility of escaping form it. In our study, we perform basin-hopping simulations with either empirical potential or DFT at 3000 K starting from either a randomly generated configuration or a known structure. A large 216-atom (3×3×3) cubic SiC supercell is employed. For each MC move, the atoms are displaced in *x*, *y*, and *z* directions with a magnitude randomly chosen between -1.0 and +1.0 Å. Local minimizations are then performed on the new configuration using the conjugate gradient (CG) scheme. If such a move leads to a lower-energy local minimum, it is accepted immediately. Otherwise, such a move will be accepted with the probability of $p = e^{-\Delta E/k_B T}$, where ΔE is the energy change of the system, and k_B is Boltzmann constant.

3.2. Empirical interatomic potential for SiC

Empirical potential development for SiC is an active area of research. To date, many parameterizations of empirical potentials for SiC have been reported in the literature [19, 45-50] and they are typically based on the general functional forms proposed by Stillinger and Weber [51], Tersoff [52], Brenner [53], and Bazant and Kaxiras [54]. It is well known that the choice of empirical potential is problem-dependent since each potential has its own strength and weakness. A recently developed environment-dependent inter-atomic potential (EDIP) for SiC [50] is chosen since it can provide a realistic description of the energetics of point and extended defects, which is particularly important for our study. We have recently implemented the EDIP potential formalism [50, 54] in Large-scale Atomic/Molecular Massively Parallel Simulator (LAMMPS) [55].

3.3. First-principles calculations

DFT calculations are performed using the Vienna *Ab initio* simulation package (VASP) [56]. The exchange-correlation functional is described within the local density approximation (LDA) [57]. The electron-ion interactions are described by the projector-augmented wave (PAW) method [58]. We use PAW pseudopotentials with valence electron configurations of $2s^2 2p^2$ for C and $3s^2 3p^2$ for Si. The cutoff energy for plane wave basis sets is set at 500 eV. For Brillouin zone sampling, a 2×2×2 Monkhorst–Pack *k*-point mesh is used for the 216-atom supercells. Our convergence tests show that such choice of cutoff energy and *k*-point mesh is sufficient to obtain fully converged results. By computing the quantum mechanical Hellmann-Feynman forces, all internal atomic positions are fully optimized using CG method until forces are less than 0.02 eV/Å. The unit cell volume and shape are hold fixed during structural relaxations.

In the present study, we assume that all defects are in their neutral charge states and calculate their defect formation energies as:

$$E_f = E_{defect} - n_{Si} m_{Si} - n_C m_C \quad (1)$$

where E_{defect} is the total energy of a supercell containing a defect. n_{i} and m_{i} denote the number and chemical potential of species i (i=Si, C), respectively. Note that while many point defects and their complexes in SiC (e.g. C vacancy and Si vacancy) have been experimentally shown to be electrically active [59, 60], the assumption of charge neutrality is quite reasonable for C interstitial clusters considered in our study. For example, previous studies found that the GS structures of both I_2 and I_4 are electrically neutral for all values of the Fermi level [28]. In addition, our previous study [29] has further shown that the GS I_3 structure is neutral for most values of the Fermi level. Here I_n denotes a carbon interstitial cluster of size n. For the chemical potentials of pure

elements, the C-rich condition is chosen [5], although our conclusions on the stability of defect clusters obviously do not depend on such a particular choice.

4. Results and Discussion

4.1. Small C interstitial clusters

The DFT calculated dissociation energies of small carbon interstitial clusters in both GS and metastable configurations are summarized in Table 1. Comparisons with previous studies [27, 28] are made, when possible. Here the dissociation energy is defined as $E_D(n) = nE_f(I_1) - E_f(I_n)$, or the energy required to fully dissociate a I_n cluster into n non-interacting C-C split interstitials in the GS tilted <001> configuration [Fig. 1(a)]. Unlike the formation energy, the dissociation energy of a defect cluster does not depend on the reference states of pure elements. For a given cluster size, the GS structure corresponds to the one with the highest E_D.

4.1.1. Carbon di-interstitials

For I_2, basin hopping with EDIP finds that the GS structure is formed by two C interstitials occupying the bond-center (BC) positions between Si and C atoms, hereinafter referred to as $(C_{BC})_2$ [Fig. 1(b)]. This finding is in agreement with previous studies [27-29]. A metastable chainlike geometry has also been identified [Fig. 1(c)], which lies 0.92 eV per cluster above the GS. Presumably, this structure can be easily formed by connecting two C split interstitials together. Furthermore, this defect may easily grow into longer chains through the capture of additional C interstitials at either end. While not found in our GS search, we have also considered the metastable $(C_{sp})_2$ configuration consisting of two neighboring C-C <001> split interstitials tilted towards

each other [Fig. 1(d)], and our calculated dissociation energy agrees well with previous calculations [27, 28].

To validate the stability of $(C_{BC})_2$, we have performed a small number of DFT-based basin hopping steps using it as the starting configuration. In addition to the chainlike structure found by EDIP, this simulation further discovers an interesting metastable structure that is only 0.78 eV per cluster above the GS. In this structure, which we refer to as $(C_{BC})_{2,tri}$ [Fig. 1(e)], two C interstitials occupying neighboring BC positions and form an isosceles triangle with a Si atom. It is worth noting that the $(C_{BC})_{2,tri}$ structure is unstable (i.e., not a local minimum) in EDIP and therefore cannot be found by basin hopping with such a potential.

4.1.2. Carbon tri-interstitials

With the addition of a single C interstitial, the PES of I_3 becomes significantly more complicated. For I_3, the GS structure predicted by basin hopping with EDIP is identical to the previously identified $(C_{BC})_3$ configuration [29], in which three C interstitials occupy BC positions and form an equilateral triangular ring parallel to the {111} plane [Fig. 2(a)]. This defect is likely responsible for the experimentally observed photoluminescence center D_{II} in SiC, as argued in our earlier study [29]. Our search with EDIP also reveals many metastable configurations including the elongated chainlike structure [Fig. 2(c)], the dual-pentagon structure [Fig. 2(d)]. The dual-pentagon structure can be formed by putting three C interstitials at the center and edge positions of a hexagonal ring within the {111} plane, dividing the ring into two pentagons and one tetragon. We have further considered the $(C_{sp})_3$ structure proposed in Ref. [28], which consists of three neighboring C split interstitials tilted towards each other [Fig. 2(e)].

From Table 1, it can be seen that the dual-pentagon structure is much more stable than chainlike and $(C_{sp})_3$ structures, although its energy remains 2.4 eV per cluster higher than that of the GS structure.

Interestingly, a close examination of the crystal structure of cubic SiC reveals that there exists an alternative configuration for $(C_{BC})_3$, which we refer to as $(C_{BC})_{3,alt}$ [Fig. 2(b)]. DFT calculations indicate that $(C_{BC})_{3,alt}$ is only 0.47 eV per cluster less stable than $(C_{BC})_3$. As will be shown later, such a metastable structure is actually an important building block of the GS structure of carbon hexa-interstitial cluster. It is possible that continuous inter-conversions between $(C_{BC})_3$ and $(C_{BC})_{3,alt}$ configurations can be one possible mechanism for the two-dimensional migration of $(C_{BC})_3$ within the {111} plane of SiC. Future studies of the energy barrier of such a diffusion mechanism would be of great interest.

It is also interesting to note that the $(C_{BC})_3$ defect bears remarkable structural similarity to the "non-compact" model of the tri-interstitial defect in Si [61]. The GS structure for I_3 in Si is a "compact" structure with tetrahedral symmetry, which is 1.4 eV more stable than the "non-compact" one. In this study, we have constructed a similar "compact" structure for I_3 in SiC by putting a C tetrahedron at a vacant C site [Fig. 2(f)]. However, such a configuration is energetically strongly unfavorable due to the over-coordination of C atoms: each C interstitial atom is coordinated by six instead of four atoms in this structure.

Starting from $(C_{BC})_3$, we have performed 100 DFT-based basin hopping steps to locally explore this important part of the PES. Surprisingly, this simulation not only discovers the $(C_{BC})_{3,alt}$ configuration that we obtain through visual inspection, but also

reveals two other highly competitive metastable structures. In one of them, the three-carbon ring is tilted from the {111} plane towards the {110} plane, and we therefore refer to it as the $(C_{BC})_{3,tilted}$ defect [Fig. 2(g)]. This structure is 1.33 eV per cluster less stable than $(C_{BC})_3$. In the other structure, referred to as $(C_{BC})_{3,fp}$ [Fig. 2(h)], the C atom above the carbon triangle in $(C_{BC})_3$ moves away from its regular lattice position and forms a C-C dumbbell with a nearby C atom, effectively forming a C Frenkel pair. Remarkably, such a structure lies only 0.38 eV per cluster above the GS. Again, similar to $(C_{BC})_{2,tri}$, it is not possible to find these energetically low-lying metastable structures without performing DFT-based simulations.

4.1.3. Carbon tetra-interstitials

For I_4, basin hopping with EDIP predicts its GS structure to be the $(C_{sp})_4$ configuration [Fig. 3(a)], which agrees with previous studies [28, 29]. In addition, our search reveals two previously unidentified metastable structures that are energetically highly competitive. One such configuration, which we refer to as $[(C_{BC})_2]_2$, consists of two parallel, non-touching $(C_{BC})_2$ defects [Fig. 3(b)]. This bound configuration is only 0.39 eV per cluster higher in energy than $(C_{sp})_4$, and can be easily formed by the agglomeration of two $(C_{BC})_2$ defects. Another metastable structure can be described as a reconstructed $(C_{sp})_4$ structure by rotating two of the C-C dumbbells, which we refer to as $(C_{sp})_{4,recon}$ [Fig. 3(d)]. Interestingly, after the bond rearrangements, all C atoms remain fourfold coordinated. This perfect coordination may explain why $(C_{sp})_{4,recon}$ is only 0.22 eV per cluster less stable than $(C_{sp})_4$.

For completeness, we have also shown in Fig. 3 two higher-energy metastable I_4 structures found in our previous study using random sampling method [29]. The tri-

pentagon structure [Fig. 3(c)] can be formed by putting four C interstitial at the center and edge positions of a hexagonal ring within the {111} plane of SiC, dividing the ring into three pentagons. This structure is almost energetically degenerate with the chainlike structure [Fig. 3(e)]. While not predicted in our study, we have also considered the $[(C_2)_{hex}]_2$ configuration [28], in which four C interstitials occupy four neighboring BC positions and form a compact rectangle within the (001) plane [Fig. 3(f)]. Interestingly, $[(C_2)_{hex}]_2$ is energetically unfavorable compared with other competing I_4 structures (Table 1), despite the fact that all atoms are fourfold coordinated in this defect. Evidently, in addition to bonding considerations, the strain energy arising from elastic interactions between a defect cluster and its surrounding matrix may also play a role in determining its GS structure.

It is reasonable to ask if $(C_{BC})_3$ can capture an additional C interstitial and transform into $(C_{sp})_4$. However, since the two structures bear no clear structural link, such a transition may necessitate the breaking of many strong covalent bonds and could thus have a high activation barrier. Furthermore, since all bonds in $(C_{BC})_3$ are already saturated [29], we expect its ability to capture an additional C interstitial to be weak. To test this hypothesis, we have constructed a I_4 structure by putting an additional C interstitial atom near the three-atom ring in $(C_{BC})_3$, which we refer to as $(C_{BC})_3$+I [Fig. 3(g)]. Interestingly, the dissociation energy of $(C_{BC})_3$+I is only 0.57 eV higher than that of $(C_{BC})_3$, suggesting that the extra C interstitial atom is not strongly bound to $(C_{BC})_3$.

For I_4, our DFT-based basin hopping simulations do not lead to the discovery of new GS or low-lying metastable structures.

4.1.4. Carbon penta- and hexa-interstitials

As far as we know, due to their extremely complex PESs, no previous reports of the GS structures of carbon penta- and hexa-interstitials exist in the literature. According to our basin-hopping search with EDIP potential, the GS structure of I_5 consists of five C interstitials occupying BC positions, forming a zigzag chain parallel to the {111} plane [Fig. 4(b)]. We therefore refer to it as $(C_{BC})_5$. By capturing two more C interstitial atoms, $(C_{sp})_{4,recon}$ can easily transform into the GS I_6 configuration in EDIP, denoted here as $(C_{sp})_{4,recon}+2I$ [Fig. 4(e)].

In view of the exceptional stability of $(C_{BC})_3$ found in our previous study [29], we have further explored the possibility that this defect cluster can be a fundamental building block of larger defects in SiC. To this end, we have constructed a I_5 structure by putting one $(C_{BC})_3$ and one $(C_{BC})_2$ defect in close proximity to each other, which we refer to as $(C_{BC})_3+(C_{BC})_2$ [Fig. 4(a)]. Interestingly, according to our DFT calculations, such a structure is actually 0.83 eV per cluster more stable than the $(C_{BC})_5$ structure, making it the true GS structure for I_5. We have tested other possibilities by placing $(C_{BC})_3$ and $(C_{BC})_2$ in different relative positions. We do not find any configuration with energy lower than the one shown in Fig. 4(a). Furthermore, we have created a similar structure by placing one $(C_{BC})_{3,alt}$ and one $(C_{BC})_2$ defect together. This defect, which we refer to as $(C_{BC})_{3,alt}+(C_{BC})_2$ [Fig. 4(c)], lies 0.60 eV per cluster above the GS.

Similarly to I_5, we have constructed various I_6 configurations using $(C_{BC})_3$ and $(C_{BC})_{3,alt}$ as building blocks. For I_6, we find that the true GS structure consists of two non-touching $(C_{BC})_3$ and $(C_{BC})_{3,alt}$ defects placed next to each other, which we call $(C_{BC})_3+(C_{BC})_{3,alt}$ [Fig. 4(d)]. DFT calculations indicate that this structure is 0.64 eV per cluster more stable than $(C_{sp})_{4,recon}+2I$. An alternative configuration of I_6 consists of two

$(C_{BC})_3$ defects at larger separations, designated as $[(C_{BC})_3]_2$ in our study [Fig. 4(f)]. This structure lies only 0.15 eV per cluster above the GS $(C_{BC})_3$+$(C_{BC})_{3,alt}$ structure. Finally, we have considered a $[(C_{BC})_2]_3$ configuration consisting of three bound $(C_{BC})_2$ defects [Fig. 4(g)]. However, this defect is energetically unfavorable compared to $(C_{BC})_3$+$(C_{BC})_{3,alt}$ and $[(C_{BC})_3]_2$.

For I_5 and I_6, our DFT-based basin hopping simulations do not find any new GS structure. It is interesting to note that the GS $(C_{BC})_3$+$(C_{BC})_2$ structure can also be found from DFT-based basin hopping using the metastable $(C_{BC})_5$ structure as the initial configuration. Admittedly, for large clusters, identifying their GS structures using DFT-based basin hopping can be a challenging task due to the large number of MC steps needed to explore their complex PESs.

4.1.5. Origin of the discrepancies between EDIP and DFT

For carbon di-, tri- and tetra-interstitial clusters in SiC, the GS structures predicted by EDIP and DFT are identical, which shows that the EDIP potential is a very good choice for studies of defects in SiC. However, if possible, predictions from empirical potentials need to be verified with more accurate quantum mechanical calculations. For instance, for both carbon penta- and hexa-interstitials, the GS structures predicted by EDIP empirical potential are actually metastable according to DFT. To gain some insight into the origin of such a discrepancy, we plot in Fig. 5 the dissociation energy per interstitial, $E_D(n)/n$, of small carbon interstitial clusters as a function of cluster size. DFT calculations employing LDA and generalized gradient approximation (GGA) of Perdew, Burke, and Ernzerhof [62] give rather similar results. For I_5 and I_6, we do not show the

EDIP results in the plot since the GS structures predicted by DFT and EDIP do not agree with each other.

According to DFT, the dissociation energy per interstitial exhibits a distinct maximum at n=3, indicating an exceptional thermodynamic stability of $(C_{BC})_3$. However, contrasting DFT results, EDIP potential predicts that C tri-interstitial cluster is much less stable than C tetra-interstitial cluster. In the $(C_{BC})_3$ defect, the three C interstitial atoms form a equilateral triangle, which requires the bond angles between C-C bonds to be 60°. Since each C atom is sp^3 hybridized, the ideal bond angle should instead be 109.5°. The large difference between the ideal and actual bond angles can lead to significant angle strain. In cyclopropane (C_3H_6) that contains a similar C triangle, the C-C bonds are bent outwards to reduce the bond strain through distorting the sp^3 hybridization of carbon atoms [63]. We expect a similar mechanism to operate in SiC, which nevertheless cannot be well treated by an empirical potential due to its quantum mechanical nature. Indeed, we find an equilateral C triangle to be energetically unfavorable in EDIP. In the GS structure of C tri-interstitial cluster in EDIP, the C triangle is actually broken (see inset in Fig. 5) in order to release the high ring strain. Presumably, this explains why EDIP drastically underestimates the stability of the $(C_{BC})_3$ defect compared with $(C_{sp})_4$. Consequently, the true GS structures of larger C interstitial clusters, which contain $(C_{BC})_3$ as a basic building block, are only favored in DFT calculations, but not by EDIP.

4.1.6. Possible mechanism for growth of C interstitial clusters in SiC

A common structural feature of the GS structures of I_2, I_3, I_5 and I_6 is that the C interstitial atoms form a single atomic layer parallel to the {111} planes in SiC. Assuming that $(C_{BC})_2$ defects are mobile, the GS I_5 structure can be easily formed from

$(C_{BC})_3$ through the capture of an additional $(C_{BC})_2$ defect, completely bypassing $(C_{sp})_4$. The binding energy between $(C_{BC})_3$ and $(C_{BC})_2$ defects, calculated as $E_b = E_f((C_{BC})_3) + E_f((C_{BC})_2) - E_f((C_{BC})_3 + (C_{BC})_2)$, is 1.43 eV. Consequently, migrating $(C_{BC})_2$ defects are strongly attracted to $(C_{BC})_3$, leading to the formation of the penta-interstitial cluster. By capturing an additional C interstitial, the bound $(C_{BC})_3$+$(C_{BC})_2$ structure can be readily transformed into $(C_{BC})_3$+$(C_{BC})_{3,alt}$, the GS structure of I_6. Although we have not calculated the reaction barrier, we expect such a reaction to be kinetically favorable since no major bond reconfiguration will be needed. Presumably, by continuous absorption of $(C_{BC})_2$ and C split interstitial defects, $(C_{BC})_3$ can grow into larger planar interstitial clusters on {111} planes. We hypothesize that this can be an important mechanism leading to the formation of the interstitial Frank loops on {111} planes observed in neutron-irradiated 3C-SiC samples by high-resolution electron microscopy [31-33].

4.2. Interactions of small C interstitial clusters with C antisite

In addition to interstitials and vacancies, antisite defects can also be created in SiC upon irradiation. A carbon antisite (C_{Si}) can act as a nucleus for larger C clusters by capturing nearby C interstitials. It is thus of interest to investigate that structure and stability of C aggregates at a vacant Si site, denoted as $(C_n)_{Si}$ in our study. Using GS search with EDIP, we have found several interesting structures of $(C_n)_{Si}$ defects. Their dissociation energies are further shown in Table 1. The dissociation energy of $(C_n)_{Si}$ is defined as $E_D = E_f(C_{Si}) + (n-1)E_f(I_1) - E_f((C_n)_{Si})$, i.e., the energy required to fully dissociate $(C_n)_{Si}$ into n-1 non-interacting C split interstitials and a C antisite.

For di- and tri-carbon antisites, basin hopping with EDIP predicts GS structures in agreement with earlier studies [27, 28]. In the GS structure of $(C_2)_{Si}$, two C atoms occupy a vacant Si site and form a dumbbell along the <001> direction [Fig. 6(a)]. In the GS structure of $(C_3)_{Si}$, three C atoms form an isosceles triangle at a vacant Si site [Fig. 6(b)]. Two of the three C atoms in the triangle forms a short C=C double bond. The previously identified square configuration [27, 28] has also been found by our basin hopping search [Fig. 6(d)]. Furthermore, our search reveals a metastable pentagon configuration [Fig. 6(c)] that has not been previously reported.

For tetra-carbon antisite $(C_4)_{Si}$, the lowest-energy structure according to basin hopping with EDIP is a dual-triangle configuration with C_s symmetry [Fig. 7(a)], which has also been reported in a previously study [28]. Such structure is 0.30 eV per cluster more stable than the symmetric tetrahedron configuration [Fig. 7(d)] with T_d symmetry. Additionally, we have identified several metastable configurations that are energetically very competitive, including a hexagon [Fig. 7(b))] and a pentagon [Fig. 7(c)] structure.

Remarkably, starting from the dual-triangle configuration of $(C_4)_{Si}$, our DFT-based basin hopping has identified a structure that is 0.58 eV per defect lower in energy. In this new GS structure, which we refer to as $(C_3)_{Si,tri}+I$ [Fig. 7(e))], three of the four C atoms form an isosceles triangle at the vacant Si site, with the fourth one forming a dumbbell with a nearby C atom. Unlike the dual-triangle configuration, all atoms in $(C_3)_{Si,tri}+I$ are fourfold coordinated (sp^3 hybridized). This true GS structure for tetra-carbon antisite is however very unstable in EDIP and therefore can only be found using DFT-based methods.

We obtain the binding energy between a C antisite and a I_n defect as $E_D = E_f(C_{Si}) + E_f(I_n) - E_f((C_{n+1})_{Si})$. For C interstitial, $(C_{BC})_2$ and $(C_{BC})_3$ defects, we calculate E_b to be 3.96, 4.16 and 3.42 eV, respectively. These large binding energies indicate that, in addition to clustering with each other, C interstitials can also get trapped at preexisting carbon antisites and form very stable complexes in SiC.

5. Summary

In this paper, we present findings of the lowest-energy configurations of small carbon interstitial clusters and carbon-antisite-based defects in technologically important 3C-SiC using a Monte-Carlo basin-hopping technique. In addition to a library of candidate structures collected from extensive basin hopping search with a recently developed EDIP potential, we have also created additional candidate GS configurations based on our physical intuitions. The stabilities of these candidate structures are then determined using DFT calculations. Finally, we have performed short DFT-based basin hopping simulations to explore the most promising region of the PES. Our approach proves to be powerful and successfully unveils many new GS as well as energetically low-lying metastable defect cluster configurations that cannot be found in our previous study. In fact, many of these structures can only be obtained from DFT calculations, but not from empirical-potential-based simulations. The present study suggests the tri-interstitial defect as an important building block of the GS structures of carbon interstitial clusters in SiC. Furthermore, this defect can be an effective nucleation site for the {111} planar interstitial clusters observed experimentally in neutron-irradiated 3C-SiC samples. The defect structures identified in the present study may also exist in other zinc-blende two-component covalent materials. Experimental identification of the defect clusters

discovered in our study, e.g., using high resolution scanning transmission electron microscopy (STEM), will be of great interest.

Acknowledgements

This research is supported by US Department of Energy, Office of Basic Energy Sciences grant DE-FG02-08ER46493.

REFERENCES

[1] Zinkle S, Busby J. Mater Today 2009;12:12.

[2] Katoh Y, Snead LL, Szlufarska I, Weber WJ. Curr Opin Solid State Mater Sci 2012;16:143.

[3] Madar R. Nature 2004;430:974.

[4] Casady JB, Johnson RW. Solid-State Electronics 1996;39:1409.

[5] Shrader D, Khalil SM, Gerczak T, Allen TR, Heim AJ, Szlufarska I, Morgan D. J Nucl Mater 2011;408:257.

[6] Ishimaru M, Bae IT, Hirotsu Y. Phys Rev B 2003;68:144102.

[7] Devanathan R, Gao F, Weber WJ. Appl Phys Lett 2004;84:3909.

[8] Ishimaru M, Bae IT, Hirata A, Hirotsu Y, Valdez JA, Sickafus KE. Phys Rev B 2005;72:024116.

[9] Ivashchenko VI, Turchi PEA, Shevchenko VI. Phys Rev B 2007;75:085209.

[10] Xue K, Niu LS. J Appl Phys 2009;106:083505.

[11] Usman M, Hallen A, Ghandi R, Domeij M. Phys Scr 2010;141:014102.

[12] de la Rubia TD, Zbib HM, Khraishi TA, Wirth BD, Victoria M, Caturla MJ. Nature 2000;406:871.

[13] Fu CC, Torre JD, Willaime F, Bocquet JL, Barbu A. Nat Mater 2005;4:68.

[14] Bai XM, Voter AF, Hoagland RG, Nastasi M, Uberuaga BP. Science 2010;327:1631.

[15] Lucas G, Pizzagalli L. Phys Rev B 2005;72:161202.

[16] Barry AL, Lehmann B, Fritsch D, Braunig D. IEEE Trans Nucl Sci 1991;38:1111.

[17] Devanathan R, Weber WJ, de la Rubia TD. Nucl Instrum Methods Phys Res B

1998;141:118.

[18] Gao F, Weber WJ. Phys Rev B 2000;63:054101.

[19] Devanathan R, de la Rubia TD, Weber WJ. J Nucl Mater 1998;253:47.

[20] Lucas G, Pizzagalli L. J Phys: Condens Matter 2007;19:086208.

[21] Roma G, Crocombette JP. J Nucl Mater 2010;403:32.

[22] Bockstedte M, Mattausch A, Pankratov O. Phys Rev B 2004;69:235202.

[23] Swaminathan N, Kamenski PJ, Morgan D, Szlufarska I. Acta Mater 2010;58:2843.

[24] Kondo S, Katoh Y, Snead LL. Phys Rev B 2004;83:075202.

[25] Ortiz CJ, Caturla MJ. Phys Rev B 2007;75:184101.

[26] Swaminathan N, Morgan D, Szlufarska I. J Nucl Mater 2011;414:431.

[27] Gali A, Deak P, Ordejon P, Son NT, Janzen E, Choyke WJ. Phys Rev B 2003;68:125201.

[28] Mattausch A, Bockstedte M, Pankratov O. Phys Rev B 2004;70:235211.

[29] Jiang C, Morgan D, Szlufarska I. Phys Rev B 2012;86:144118.

[30] Gao F, Weber WJ, Posselt M, Belko V. Phys Rev B 2004;69:245205.

[31] Yano T, Suzuki T, Maruyama T, Iseki T. J Nucl Mater 1988;155:311.

[32] Yano T, Iseki T. Philos Mag A 1990;62:421.

[33] Katoh Y, Hashimoto N, Kondo S, Snead LL, Kohyama A. J Nucl Mater 2006;351:228.

[34] Ballone P, Milani P. Phys Rev B 1990;42:3201.

[35] Jones RO. Phys Rev Lett 1991;67:224.

[36] Binggeli N, Martins JL, Chelikowsky JR. Phys Rev Lett 1992;68:2956.

[37] Pickard CJ, Needs RJ. Phys Rev Lett 2006;97:045504.

[38] Jiang C, Lin ZJ, Zhao YS. Phys Rev Lett 2009;103:185501.

[39] Martinez-Canales M, Pickard CJ, Needs RJ. Phys Rev Lett 2012;108:045704.

[40] Ballone P, Andreoni W, Car R, Parrinello M. Phys Rev Lett 1988;60:271.

[41] Kawai R, Weare JH. Phys Rev Lett 1990;65:80.

[42] Hartke B, Carter EA. Chem Phys Lett 1993;216:324.

[43] Wales DJ, Doye JPK. J Phys Chem A 1997;101:5111.

[44] Wales DJ, Scheraga HA. Science 1999;285:1368.

[45] Tersoff J. Phys Rev B 1994;49:16349.

[46] Dyson AJ, Smith PV. Surf Sci 1996;355:140.

[47] Gao F, Weber WJ. Nucl Instrum Methods Phys Res B 2002;191:504.

[48] Erhart P, Albe K. Phys Rev B 2005;71:035211.

[49] Vashishta P, Kalia RK, Nakano A, Rino JP. J Appl Phys 2007;101:103515.

[50] Lucas G, Bertolus M, Pizzagalli L. J Phys: Condens Matter 2010;22:035802.

[51] Stillinger FH, Weber TA. Phys Rev B 1985;31:5262.

[52] Tersoff J. Phys Rev B 1988;37:6991.

[53] Brenner DW. Phys Rev B 1990;42:9458.

[54] Bazant M, Kaxiras E. Phys Rev Lett 1996;77:4370.

[55] Plimpton S. J Comp Phys 1995;117:1.

[56] Kresse G, Furthmuller J. Phys Rev B 1996;54:11169.

[57] Ceperly DM, Alder BJ. Phys Rev Lett 1980;45:566.

[58] Kresse G, Jouber D. Phys Rev B 1999;59:1758.

[59] Son NT, Hai PN, Janzen E. Phys Rev B 2001;63:201202.

[60] Son NT, Carlsson P, ul Hassan J, Magnusson B, Janzen E. Phys Rev B 2007;75:155204.

[61] Lopez GM, Fiorentini V. J Phys: Condens Matter 2003;15:7851.

[62] Perdew JP, Burke K, Ernzerhof M. Phys Rev Lett 1996;77:3865.

[63] Wiberg KB. Acc Chem Res 1996;29:229.

TABLE 1. First-principles calculated cluster dissociation energies (eV per defect cluster) of small carbon interstitial clusters (I_n) in 3C-SiC. Results for small C clusters at a vacant Si site, $(C_n)_{Si}$, are also shown. Defects in the neutral charge state are considered.

Defect type	n	Cluster structure	This study	Ref. [28]	Ref. [27]
I_n	2	$(C_{BC})_2$	5.16	4.8	5.3
		Chainlike	4.25	-	-
		$(C_{sp})_2$	2.81	2.8	2.9
		$(C_{BC})_{2,tri}$	4.39	-	-
	3	$(C_{BC})_3$	9.52	-	-
		$(C_{BC})_{3,alt}$	9.05	-	-
		Chainlike	5.66	-	-
		Dual-Pentagon	7.10	-	-
		$(C_{sp})_3$	5.83	5.8	-
		Tetrahedron	0.94	-	-
		$(C_{BC})_{3,tilted}$	8.19	-	-
		$(C_{BC})_{3,fp}$	9.14	-	-
	4	$(C_{sp})_4$	12.37	11.5	-
		$[(C_{BC})_2]_2$	11.97	-	-
		Tri-Pentagon	10.76	-	-
		$(C_{sp})_{4,recon}$	12.15	-	-
		Chainlike	10.67	-	-
		$[(C_2)_{hex}]_2$	10.09	9.2	-
		$(C_{BC})_3$+I	10.09	-	-
	5	$(C_{BC})_3$+$(C_{BC})_2$	16.12	-	-
		$(C_{BC})_5$	15.29	-	-
		$(C_{BC})_{3,alt}$+$(C_{BC})_2$	15.52	-	-
	6	$(C_{BC})_3$+$(C_{BC})_{3,alt}$	19.46	-	-
		$(C_{sp})_{4,recon}$+2I	18.81	-	-
		$[(C_{BC})_3]_2$	19.31	-	-
		$[(C_{BC})_2]_3$	18.73	-	-
$(C_n)_{Si}$	2	Dumbbell	3.96	4.1	3.9
	3	Triangle	9.32	8.9	-
		Pentagon	6.28	-	-
		Square	7.95	7.7	7.9
	4	Dual-Triangle	12.36	11.7	-
		Hexagon	11.64	-	-
		Pentagon	11.79	-	-
		Tetrahedron	12.07	-	-
		$(C_3)_{Si,tri}$+I	12.94	-	-

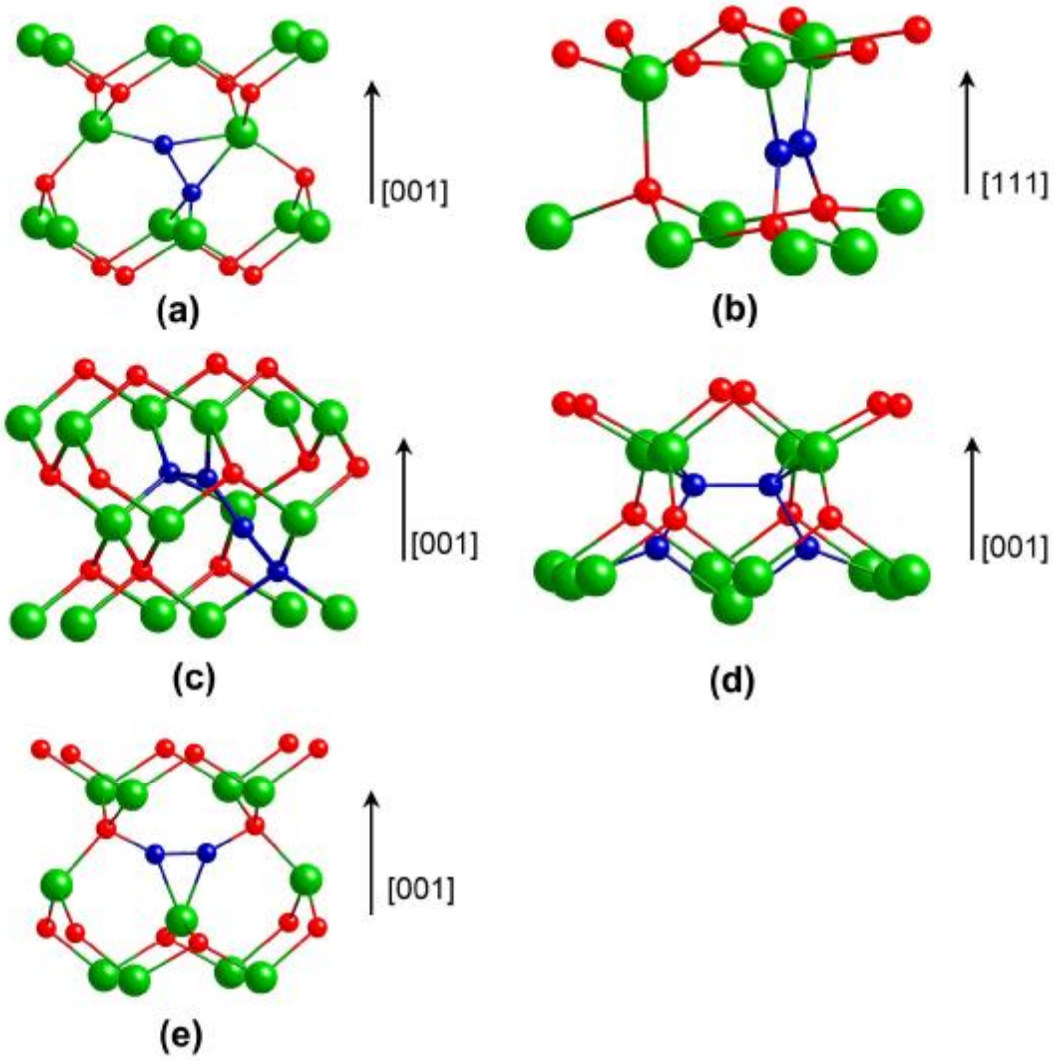

FIG. 1 C mono- and di-interstitial defects in 3C-SiC: (a) tilted <001> split interstitial, (b) $(C_{BC})_2$, (c) chainlike I_2, (d) $(C_{sp})_2$, and (e) $(C_{BC})_{2,tri}$. Large and small spheres represent Si and C atoms, respectively.

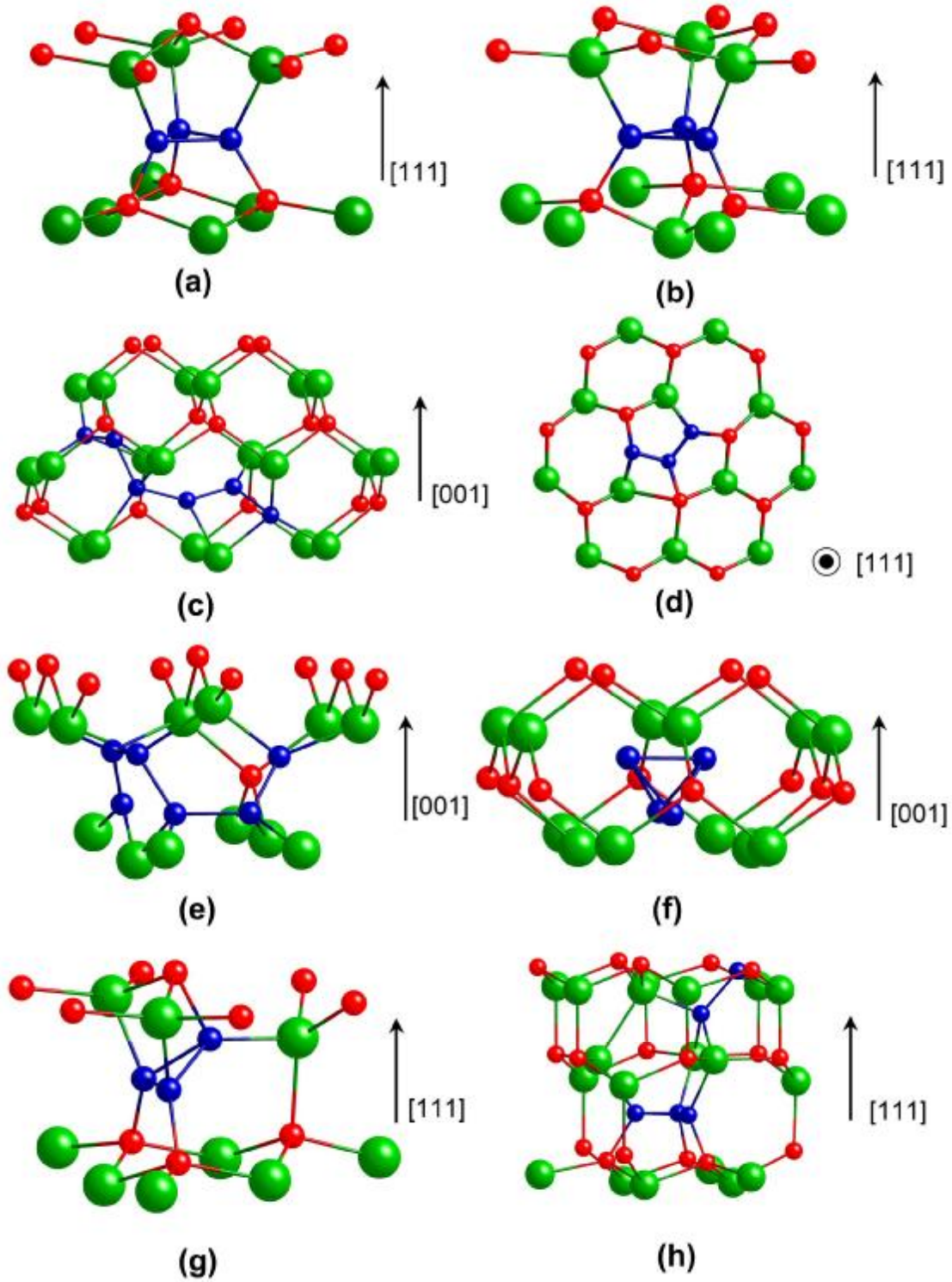

FIG. 2 C tri-interstitial defects in 3C-SiC: (a) $(C_{BC})_3$, (b) $(C_{BC})_{3,alt}$, (c) chainlike, (d) dual-pentagon, (e) $(C_{sp})_3$, (f) tetrahedron, (g) $(C_{BC})_{3,tilted}$, and (h) $(C_{BC})_{3,fp}$. Large and small spheres represent Si and C atoms, respectively.

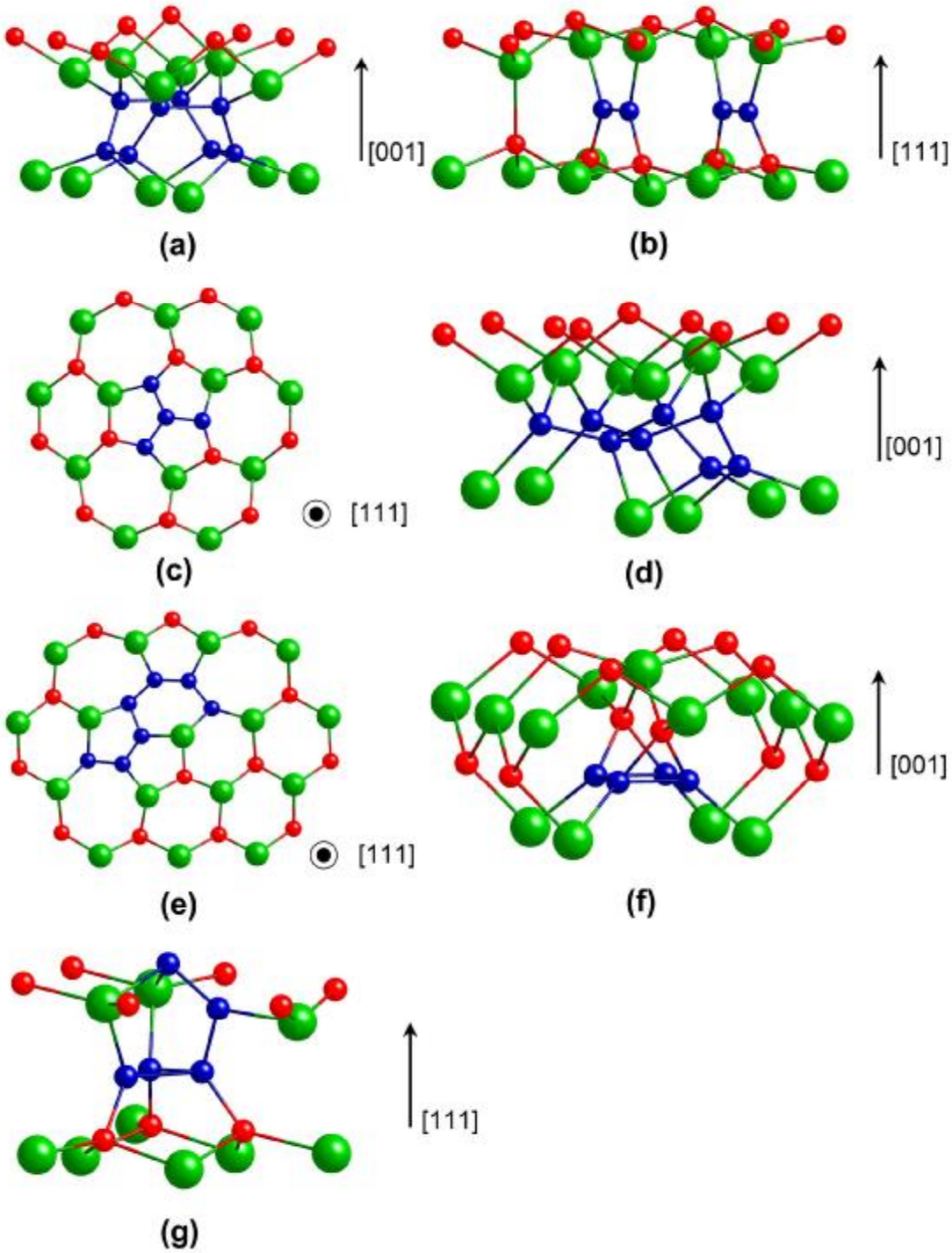

FIG. 3 C tetra-interstitial defects in 3C-SiC: (a) $(C_{sp})_4$, (b) $[(C_{BC})_2]_2$, (c) tri-pentagon, (d) reconstructed $(C_{sp})_4$, (e) chainlike, (f) $[(C_2)_{hex}]_2$, and (g) $(C_{BC})_3$+*I*. Large and small spheres represent Si and C atoms, respectively.

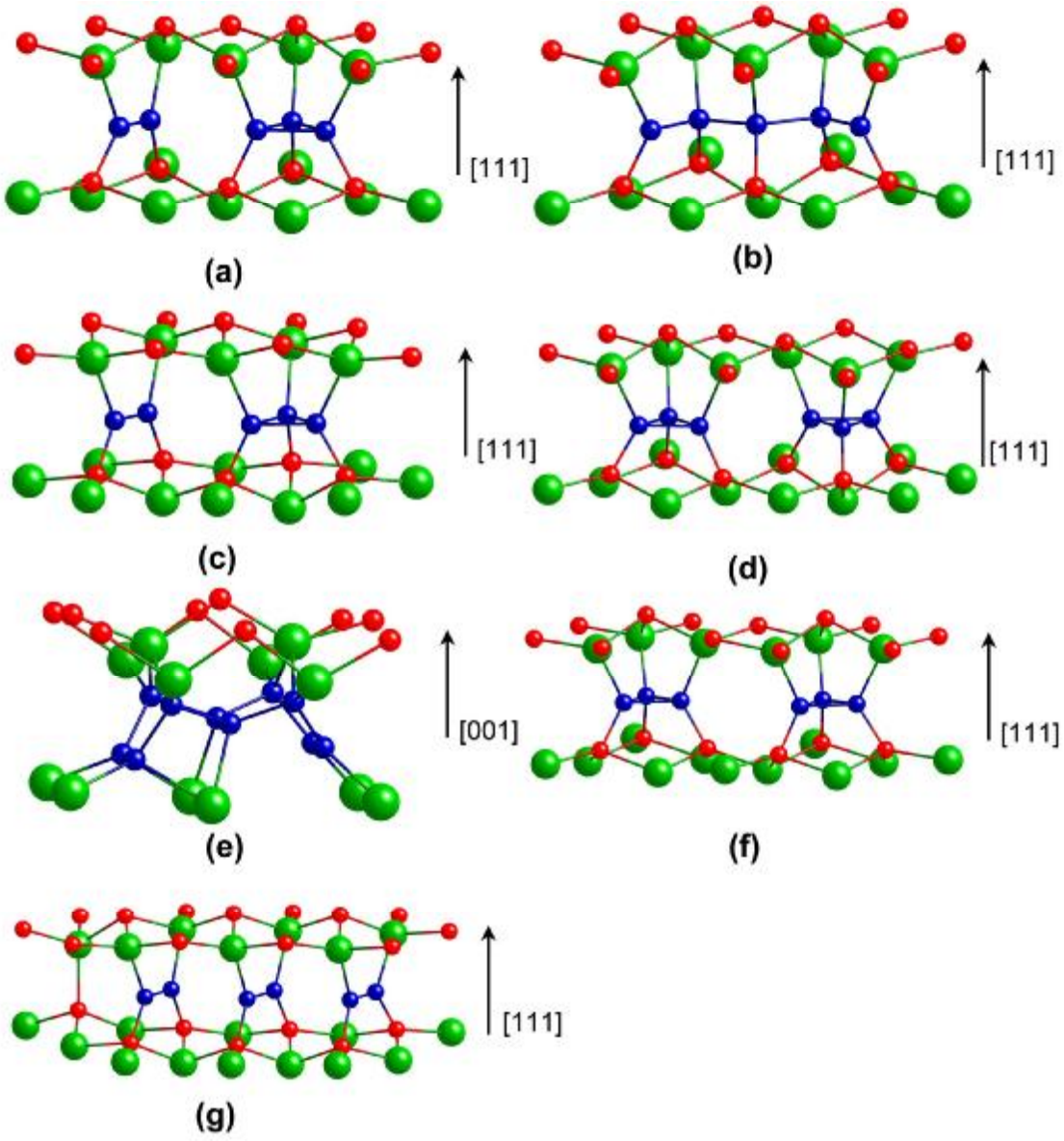

FIG. 4 C penta- and hexa-interstitial defects in 3C-SiC: (a) $(C_{BC})_3+(C_{BC})_2$, (b) $(C_{BC})_5$, (c) $(C_{BC})_{3,alt}+(C_{BC})_2$, (d) $(C_{BC})_3+(C_{BC})_{3,alt}$, (e) $(C_{sp})_{4,recon}+2I$, (f) $[(C_{BC})_3]_2$, and (g) $[(C_{BC})_2]_3$. Large and small spheres represent Si and C atoms, respectively.

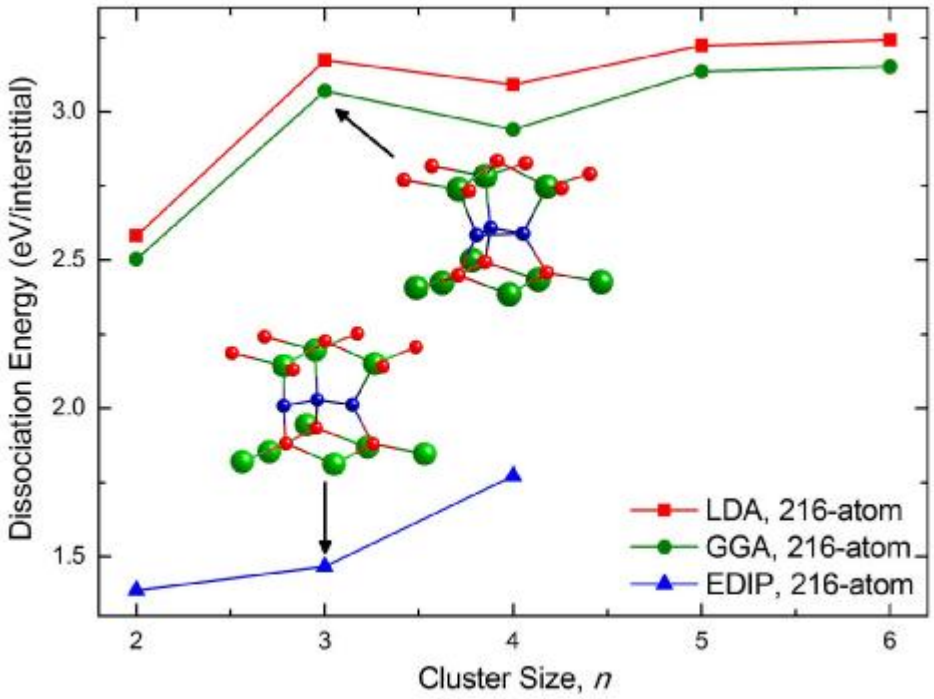

FIG. 5 Dissociation energies (per interstitial) of small carbon interstitial clusters in their ground state structures as a function of cluster size. Both results calculated using DFT and EDIP are shown. The ground state structures of C tri-interstitial cluster predicted by DFT and EDIP are shown as insets.

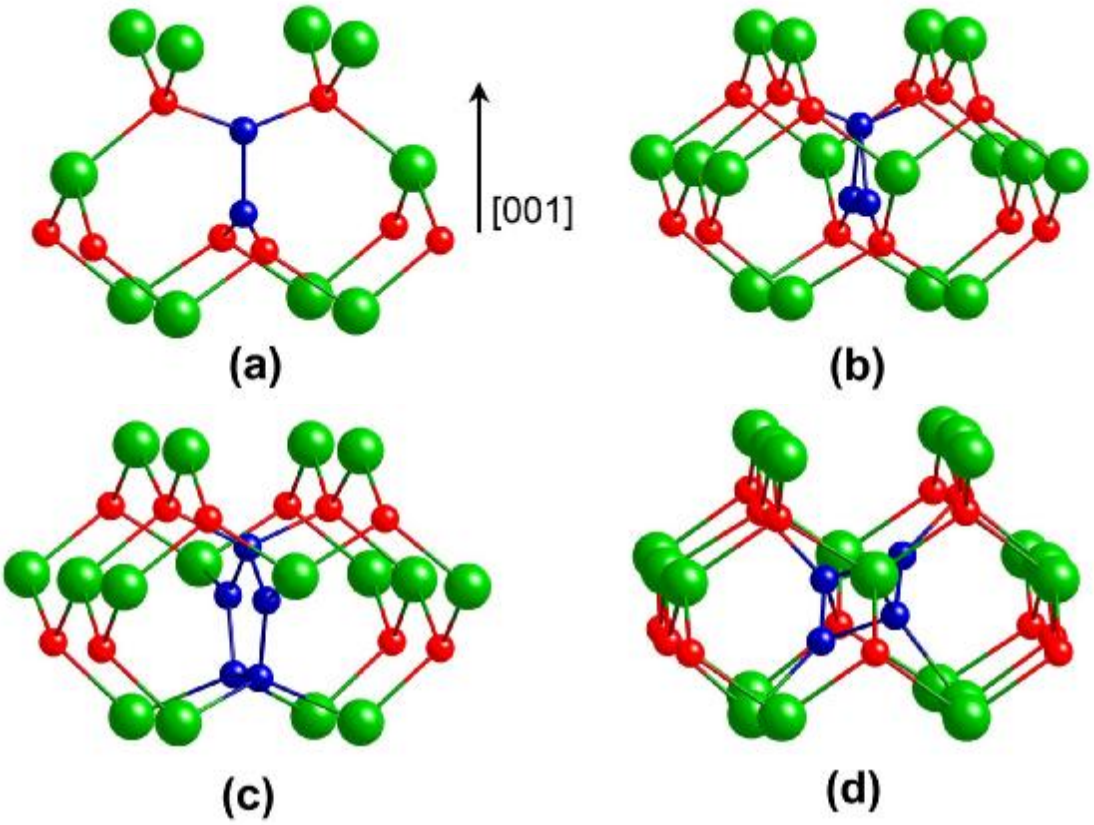

FIG. 6 Di- and tri-carbon antisites in SiC: (a) dumbbell, (b) triangle, (c) pentagon, and (d) square. Large and small spheres represent Si and C atoms, respectively.

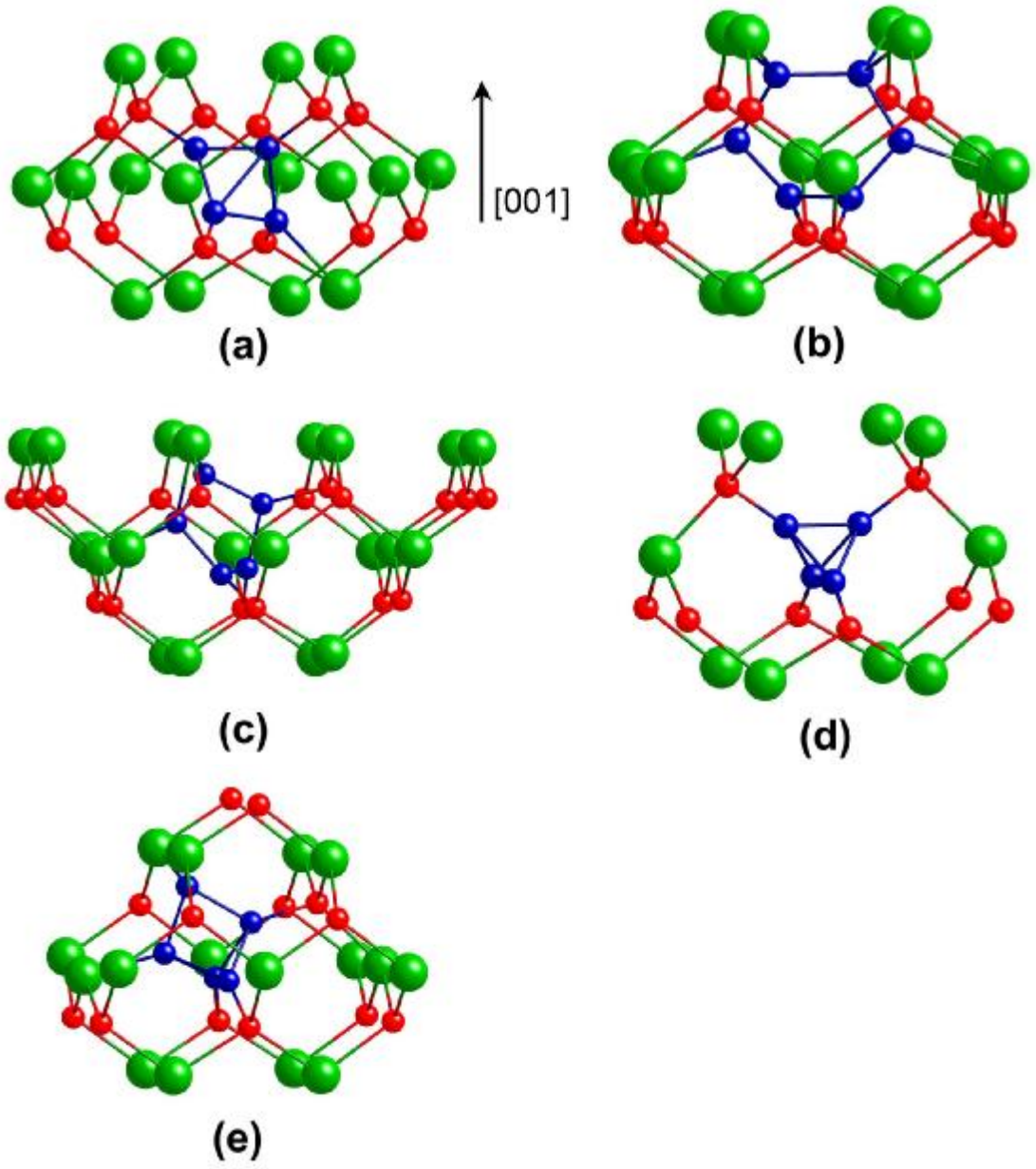

FIG. 7 Tetra-carbon antisites in SiC: (a) dual-triangle, (b) hexagon, (c) pentagon, (d) tetrahedron, and (e) $(C_3)_{Si,tri}$+*I*. Large and small spheres represent Si and C atoms, respectively.